

Half-Metallic Superconducting Triplet Spin Valve

Klaus Halterman^{1,*} and Mohammad Alidoust^{2,†}

¹*Michelson Lab, Physics Division, Naval Air Warfare Center, China Lake, California 93555*

²*Department of Physics, Faculty of Sciences, University of Isfahan, Hezar Jerib Avenue, Isfahan 81746-73441, Iran*
(Dated: July 15, 2016)

We theoretically study a finite size SF_1NF_2 spin valve, where a normal metal (N) insert separates a thin standard ferromagnet (F_1) and a thick half-metallic ferromagnet (F_2). For sufficiently thin superconductor (S) widths close to the coherence length ξ_0 , we find that changes to the relative magnetization orientations in the ferromagnets can result in substantial variations in the transition temperature T_c , consistent with experiment [Singh *et al.*, *Phys. Rev. X* **5**, 021019 (2015)]. Our results demonstrate that, in good agreement with the experiment, the variations are largest in the case where F_2 is in a half-metallic phase and thus supports only one spin direction. To pinpoint the origins of this strong spin-valve effect, both the equal-spin f_1 and opposite-spin f_0 triplet correlations are calculated using a self-consistent microscopic technique. We find that when the magnetization in F_1 is tilted slightly out-of-plane, the f_1 component can be the dominant triplet component in the superconductor. The coupling between the two ferromagnets is discussed in terms of the underlying spin currents present in the system. We go further and show that the zero energy peaks of the local density of states probed on the S side of the valve can be another signature of the presence of superconducting triplet correlations. Our findings reveal that for sufficiently thin S layers, the zero energy peak at the S side can be larger than its counterpart in the F_2 side.

PACS numbers: 74.45.+c, 74.78.Fk, 75.70.-i

In the field of superconducting spintronics, there is interest in spin-controlled proximity effects for manipulating the superconductivity in ferromagnet (F) and superconductor (S) layered systems [1, 2]. When an S layer is in contact with two ferromagnets, creating a superconducting spin valve, the superconducting state can be controlled by changing the relative magnetization directions [3–5]. The basic superconducting spin-valve involves SFF structures [3, 6] where switching between relative parallel and antiparallel magnetizations modifies the oscillatory singlet pairing in the F regions. For strong ferromagnets, these oscillations have limited extent, as they become damped out over very short distances [7]. If however, the mutual magnetizations vary noncollinearly, the broken time reversal and translation symmetries induces a mixture of spin singlet and odd-frequency (or odd-time) spin-triplet correlations with 0 and ± 1 spin projections along the magnetization axis [8, 9]. The triplet pairs with nonzero spin projection can naturally penetrate extensively within the ferromagnet layers [10–16] and result in an enhancement of the DOS at low energies [17, 18]. This long-range triplet component in SF_1F_2 type spin valves can be manipulated by changing the relative orientations of the magnetizations in F_1 and in F_2 , which creates opportunities for the development of new types of spin-valves and switches for nonvolatile memory applications [19–21]. Because of their simplicity in pinpointing fundamental phenomena and promising prospects in spintronics devices, the SF_1F_2 spin valve continues to attract broad interest [3, 6, 14, 21–25, 27, 30]. For ex-

ample, an anomalous Meissner effect has recently been observed [31] that is consistent with the generation of an odd-frequency superconducting state [32].

Recent experiments involving superconducting spin valves have investigated variations in the critical temperature, T_c [33, 34] when varying the relative in-plane magnetization angle. The suppression in T_c for nearly orthogonal magnetizations reflects the increased presence of equal-spin triplet pairs [6]. A spin valve like effect was also experimentally realized [23, 35] in FeV superlattices, where antiferromagnetic coupling between the Fe layers permits gradual rotation of the relative magnetization direction in the F_1 and F_2 layers. Most experiments involve standard ferromagnets, leading to ΔT_c sensitivity of several mK. When the outer F_2 layer is replaced by a half-metallic ferromagnet, such as CrO_2 , a very large ΔT_c has been reported, which is indicative of the presence of odd-frequency triplet superconducting correlations [25].

Besides through studying T_c , the existence and type of superconducting correlations in superconducting spin-valves can be identified through signatures of the proximity-induced electronic density of states (DOS) [26]. When triplet correlations are present in an F layer, it has been shown that a zero energy peak (ZEP) in the DOS can arise [27, 28]. The situation where pair correlations from both the spin-0 and spin-1 triplet channels are present can however make its unambiguous detection difficult. Nonetheless, this difficulty can be alleviated if one of the F layers is half-metallic (supporting one spin direction), creating an effective spin-filter that can isolate the spin-1 triplet component due to the large exchange splitting present. Thus it is of interest to investigate SF_1F_2 structures containing a half-metallic ferromagnet, where the modified triplet proximity effects can result in

* klaus.halterman@navy.mil

† phymalidoust@gmail.com

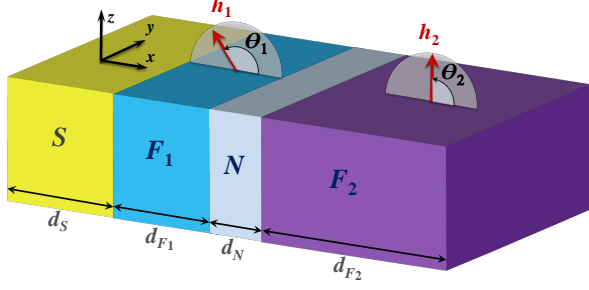


FIG. 1. (Color online). Schematic of the finite size SF_1NF_2 multilayer, where θ_1 and θ_2 characterize the magnetization orientation of ferromagnets F_1 and F_2 with thicknesses d_{F_1} and d_{F_2} , respectively. The normal metal (N) insert with thickness d_N is a nonmagnetic layer such as Cu. The exchange field in each magnet is written $\mathbf{h}_i = h_i(\cos \theta_i, 0, \sin \theta_i)$, for $i = 1, 2$. Here, θ_i is measured relative to the x -axis. The ferromagnet F_2 is half-metallic (e.g., CrO_2) so that $|\mathbf{h}_2| = E_F$, and its magnetization is fixed along the z direction ($\theta_2 = \pi/2$), whereas the magnetization in F_1 can rotate in the $x-z$ plane. We thus define the angle θ to describe the out-of-plane relative magnetization between the two magnets, with $\theta \equiv \theta_1 - \theta_2$.

strong spin valves with high sensitivity to magnetization changes and a corresponding T_c suppression.

To realistically and accurately model these systems, where $h \simeq E_F$, we use a fully microscopic microscopic framework, the Bogoliubov-de Gennes (BdG) equations, to determine the singlet and triplet pair correlations self-consistently. This approach naturally supports the study of a broad range of intermediate ferromagnetic exchange energies, including the half metallic phase, by simply setting the exchange field value close to the Fermi energy. The half metallic regime is also accessible within the quasichlassical approximation [29, 30] by considering the case when the energy splitting of the the spin-up and spin-down bands greatly exceed the Fermi energy, i.e., $h \gg E_F$. Using the BdG formalism, we show how to identify the existence of the equal-spin triplet components by probing the S side of the proposed valve with an STM, revealing signatures in the form of peaks in the density of states (DOS) at zero energy [22, 27].

I. METHODS

A schematic of the spin valve configuration is depicted in Fig. 1. We model the nanostructure as a SF_1NF_2 layered system, where S represents the superconducting layer, N denotes the normal metallic intermediate layer, and F_1 , F_2 are the inner (free) and outer (pinned) magnets, respectively. The layers are assumed to be infinite in the $y-z$ plane with a total thickness d in the x direction, which is perpendicular to the interfaces between layers. The ferromagnet F_2 has width d_{F_2} , and fixed direction of magnetization along z , while the free magnetic layer F_1 of width d_{F_1} has a variable magnetization direction. The superconducting layer of thickness d_S is in

contact with the free layer. The magnetizations in the F layers are modeled by effective Stoner-type exchange fields $\mathbf{h}(x)$ which vanish in the non-ferromagnetic layers.

To accurately describe the physical properties of our systems with sizes in the nanometer scale and over a broad range of exchange fields, where quasichlassical approximations are limited, we numerically solve the microscopic BdG equations within a fully self-consistent framework. The general spin-dependent BdG equations for the quasiparticle energies, ε_n , and quasiparticle wavefunctions, $u_{n\sigma}, v_{n\sigma}$ is written:

$$\begin{pmatrix} \mathcal{H}_0 - h_z & -h_x & 0 & \Delta(x) \\ -h_x & \mathcal{H}_0 + h_z & -\Delta(x) & 0 \\ 0 & -\Delta(x) & -(\mathcal{H}_0 - h_z) & -h_x \\ \Delta(x) & 0 & -h_x & -(\mathcal{H}_0 + h_z) \end{pmatrix} \times \begin{pmatrix} u_{n\uparrow} \\ u_{n\downarrow} \\ v_{n\uparrow} \\ v_{n\downarrow} \end{pmatrix} = \varepsilon_n \begin{pmatrix} u_{n\uparrow} \\ u_{n\downarrow} \\ v_{n\uparrow} \\ v_{n\downarrow} \end{pmatrix}, \quad (1)$$

where h_i ($i = x, z$) are components of the exchange field. In Eqs. (1), the single-particle Hamiltonian $\mathcal{H}_0 = -1/(2m)d^2/dx^2 - E_F + U(x)$ contains the Fermi energy, E_F , and an effective interfacial scattering potential described by delta functions of strength H_j (j denotes the different interfaces), namely: $U(x) = H_1\delta(x - d_S) + H_2\delta(x - d_S - d_{F_1}) + H_3\delta(x - d_S - d_{F_1} - d_N)$, where $H_j = k_F H_{Bj}/m$ is written in terms of the dimensionless scattering strength H_{Bj} . We assume $h_{x,i} = h_i \cos \theta_i$ and $h_{z,i} = h_i \sin \theta_i$ in F_i , where h_i is the magnitude of exchange field, and i denotes the region. To minimize the free energy of the system at temperature T , the singlet pair potential $\Delta(x)$ is calculated self-consistently [36]:

$$\Delta(x) = \frac{g(x)}{2} \sum_n [u_{n\uparrow}(x)v_{n\downarrow}(x) + u_{n\downarrow}(x)v_{n\uparrow}(x)] \tanh\left(\frac{\varepsilon_n}{2T}\right), \quad (2)$$

where the sum is over all eigenstates with ε_n that lie within a characteristic Debye energy ω_D , and $g(x)$ is the superconducting coupling strength, taken to be constant in the S region and zero elsewhere. The pair potential gives direct information regarding superconducting correlations within the S region only, since it vanishes in the remaining spin valve regions where $g(x) = 0$. Greater insight into the singlet superconducting correlations throughout the structure, and the extraction of the proximity effects is most easily obtained by considering the pair amplitude, f_3 , defined as $f_3 \equiv \Delta(x)/g(x)$.

To analyze the correlation between the behavior of the superconducting transition temperatures and the existence of odd triplet superconducting correlations in our system, we compute the induced triplet pairing amplitudes which we denote as f_0 (with $m = 0$ spin projection) and f_1 (with $m = \pm 1$ spin projection) according to the following equations [16]:

$$f_0(x, t) = \frac{1}{2} \sum_n [u_{n\uparrow}(x)v_{n\downarrow}(x) - u_{n\downarrow}(x)v_{n\uparrow}(x)] \zeta_n(t), \quad (3a)$$

$$f_1(x, t) = -\frac{1}{2} \sum_n [u_{n\uparrow}(x)v_{n\uparrow}(x) + u_{n\downarrow}(x)v_{n\downarrow}(x)] \zeta_n(t), \quad (3b)$$

where $\zeta_n(t) \equiv \cos(\varepsilon_n t) - i \sin(\varepsilon_n t) \tanh(\varepsilon_n/(2T))$, and t is the time difference in the Heisenberg picture. These triplet pair amplitudes are odd in t and vanish at $t = 0$, in accordance with the Pauli exclusion principle. The quantization axis in Eqs. (3a) and (3b) is along the z direction. When studying the triplet correlations in F_1 , we align the quantization axis with the local exchange field direction, so that after rotating, the triplet amplitudes f_0 and f_1 become linear combinations of the f_0 and f_1 in the original unprimed system [27]: $f'_0(x, t) = f_0(x, t) \cos \theta - f_1(x, t) \sin \theta$, and $f'_1(x, t) = f_0(x, t) \sin \theta + f_1(x, t) \cos \theta$. Thus, when the exchange fields in F_1 and F_2 are orthogonal ($\theta = \pi/2$), the roles of the equal-spin and opposite-spin triplet correlations are reversed. The singlet pair amplitude however is naturally invariant under these rotations.

The study of single-particle excitations in these systems can reveal important signatures in the proximity induced singlet and triplet pair correlations. A useful experimental tool that probes these single-particle states is tunneling spectroscopy, where information measured by a scanning tunneling microscope (STM) can reveal the local DOS, $N(x, \varepsilon)$, as a function of position x and energy ε . We write $N(x, \varepsilon)$ as a sum of each spin component ($\sigma = \uparrow, \downarrow$) to the DOS: $N(x, \varepsilon) = N_\uparrow(x, \varepsilon) + N_\downarrow(x, \varepsilon)$, where,

$$N_\sigma(x, \varepsilon) = \sum_n [u_{n\sigma}^2(x) \delta(\varepsilon - \varepsilon_n) + v_{n\sigma}^2(x) \delta(\varepsilon + \varepsilon_n)]. \quad (4)$$

II. RESULTS

We now proceed to present the self-consistent numerical results for the transition temperature, triplet amplitudes, and local DOS for the spin-valve structure depicted in Fig. 1. We normalize the temperature in the calculations by T_0 , the transition temperature of a pure bulk S sample. When in the low- T limit, we take $T = 0.05T_0$. All length scales are normalized by the Fermi wavevector k_F , so that the coordinate x is written $X = k_F x$, and the F_1 and F_2 widths are written $D_{F_i} = k_F d_{F_i}$, for $i = 1, 2$. The thick half-metallic ferromagnet F_2 has width $D_{F_2} = 400$, and F_1 is a standard ferromagnet with $h_1 = 0.1E_F$. We set $d_{F_1} = \xi_F$, where $\xi_F = v_F/(2h_1)$ is the length scale describing the propagation of spin-0 pairs. In dimensionless units we thus have, $D_{F_1} = (h_1/E_F)^{-1} = 10$, which optimizes spin mixing of superconducting correlations in the system. The S width is normalized similarly by $D_S = k_F d_S$, and its scaled coherence length is taken to be $k_F \xi_0 = 100$. Natural units, e.g., $\hbar = k_B = 1$, are used throughout.

A. Critical Temperature and Triplet Correlations

We first study the critical temperature of the spin valve system. The linearized self-consistency expression near

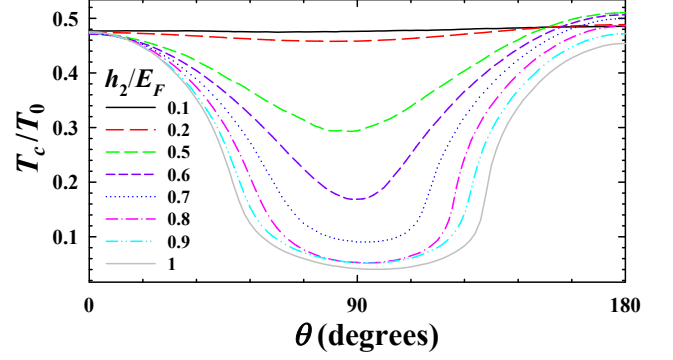


FIG. 2. (Color online). Critical temperature T_c as a function of the relative exchange field orientation angle θ at differing values of the ratio of the exchange field in the F_2 region, h_2 to the Fermi energy E_F . The legend depicts the range of h_2/E_F considered, ranging from a relatively weak ferromagnet with $h_2/E_F = 0.1$, to a fully spin polarized half-metallic phase, corresponding to $h_2/E_F = 1$.

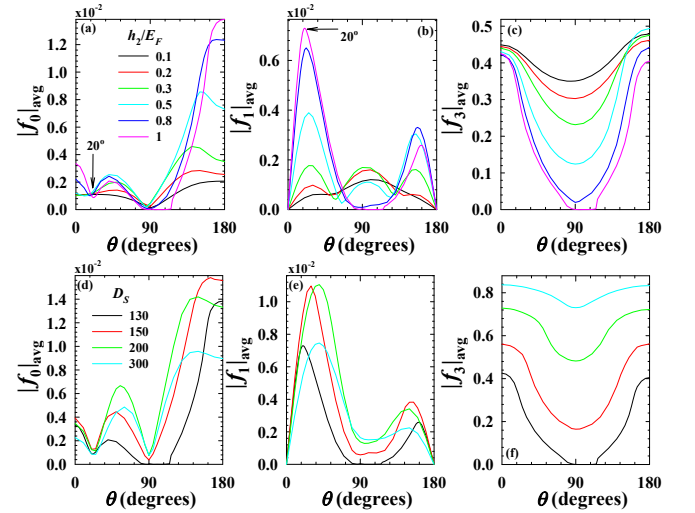


FIG. 3. (Color online). The magnitudes of the normalized triplet (f_0, f_1) and singlet (f_3) components are shown averaged over the S region and plotted as a function of the relative magnetization angle θ . The temperature is set at $T = 0.05T_0$. The top panels (a)-(c) depict differing values of the exchange field in the F_2 region as shown. All other system parameters are the same as those used in Fig. 2. Panels (d)-(f) correspond to F_2 with an optimal exchange field of $h_2/E_F = 1$, and various S widths, as labeled.

T_c takes the form, $\Delta_i = \sum_q \mathcal{G}_{iq} \Delta_q$, where Δ_i are the expansion coefficients for $\Delta(x)$ in the chosen basis. The \mathcal{G}_{iq} are the corresponding matrix elements, which involve sums of the normal state energies and wavefunctions. To determine T_c , we compute the eigenvalues λ , of the corresponding eigensystem $\mathbf{\Delta} = \lambda \mathbf{\mathcal{G}} \mathbf{\Delta}$. When $\lambda > 1$ at a given temperature, the system is in the superconducting state. Many of the computational details can be found

in Ref. 33, and are omitted here.

It was experimentally observed [25] that a SF_1F_2 spin valve is most effective at converting singlet Cooper pairs to spin polarized triplet pairs when F_2 is in a half-metallic phase. To examine this theoretically, we investigate the critical temperature and corresponding triplet pair generation as a function of h_2/E_F and θ ($h_1/E_F = 0.1$ remains fixed). The width of the superconducting layer is maintained at $D_S = 130$, and the nonmagnetic insert has a set width corresponding to $D_N = 5$. The exchange field h_2 varies from $0.1E_F$ to E_F where $h_2 = E_F$ corresponds to the situation where only one spin species exists in this region (i.e. the half-metallic phase). As seen in Fig. 2, T_c is nearly constant over the full range of θ when both ferromagnets are of the same type, i.e., when $h_2/E_F = 0.1$. Upon increasing h_2 towards the half-metallic limit, it is apparent that the spin valve effect becomes dramatically enhanced, whereby rapid changes in T_c occur when varying θ . This result therefore clearly supports the assertion that the use of a half-metal generates the most optimal spin-valve effectiveness [25]. Large variations in T_c have also been found using a diffusive quasiclassical approach involving SF_1F_2 heterostructures lacking the normal layer insert [3, 30]. When comparing T_c in the two collinear magnetic orientations, the self-consistently calculated critical temperatures in Fig. 2 reveal that the parallel state ($\theta = 0^\circ$) has a smaller T_c compared to the antiparallel state ($\theta = 180^\circ$) for moderate exchange field strengths. For these cases, the two magnets can counter one another, leading to a reduction of their effective pair-breaking effects. This creates a more favorable situation for the superconducting state, causing T_c to be larger. The situation reverses for stronger magnets with $h \gtrsim 0.8$, and the maximum T_c now arises for parallel relative orientations of the magnetizations. In between the parallel and antiparallel states, T_c undergoes a minimum that occurs not at the orthogonal orientation ($\theta = 90^\circ$), but slightly away from it. This behavior has been observed in ballistic [5] and diffusive [3] systems where the minimum in T_c arises from the leakage of Cooper pairs that are coupled to the outer F layer via the generation of the triplet component f_1 that is largest near $\theta = 90^\circ$.

To demonstrate the correlation between the strong T_c variations and the generation of triplet and singlet pairs, Fig. 3 shows the magnitudes of the equal-spin triplet amplitudes (f_1), opposite-spin triplet amplitudes (f_0), and the singlet pair amplitudes (f_3), each averaged over the S region. For the triplet correlations, a representative value for the normalized relative time τ is set at $\tau \equiv \omega_D t = 4$. When the ferromagnet (F_2) possesses a large exchange field, and the relative magnetization angle between F_1 and F_2 approaches an orthogonal state, superconductivity becomes severely weakened. Indeed, as Fig. 2 demonstrated, the singlet pair correlations can become completely destroyed at low temperatures ($T \simeq 0.05$), and orientations in the vicinity of $\theta \simeq 90^\circ$, whereby the system has transitioned to a normal resistive state. This is consistent with Fig. 3(c), where the f_3 amplitudes van-

ish in the neighborhood of $\theta \approx 90^\circ$ and $h_2/E_F = 1$. As Fig. 3(a) and (b) illustrates, the triplet amplitudes also vanish due to the absence of singlet correlations at those orientations. For weaker magnets however, the superconducting state never transitions to a normal resistive state over the entire range of θ , and the well known situation arises whereby the equal-spin triplet pairs are largest for orthogonal magnetization configurations, i.e., when the misalignment angle is greatest ($\theta \simeq 90^\circ$). In all cases however, the f_1 components must always vanish at $\theta = 0$ and $\theta = 180^\circ$, where the relative collinear magnetization alignments are either in the parallel or antiparallel state respectively. It is clear from Figs. 3(a) and 3(b) that the average behavior of $|f_0|$ and $|f_1|$ exhibits their most extreme values when T_c undergoes its steepest variations around $\theta \approx 20^\circ$ [see Fig. 2]. In particular, at the half-metallic phase, f_1 is greatly enhanced while f_0 is dramatically suppressed. Therefore, the considerable variations in T_c is correlated with the fact that 100% spin-polarized compounds such as CrO_2 result in the optimal generation of spin triplet correlations [25]. The suppression of f_0 at $\theta \approx 20^\circ$ is fairly robust to changes in the size of the S region. As the bottom panels in Figs. 3 illustrate, increasing D_S by several coherence lengths causes very little change in the location of the first minimum in f_0 at $\theta \approx 20^\circ$. The angle θ that corresponds to a peak in f_1 however, noticeably shifts to larger θ , so that at $\theta \approx 20^\circ$, f_1 is no longer at its peak value. Therefore, the thinnest S layer width considered here, $D_S = 130$, leads to the most favorable conditions for the generation of f_1 triplet pairs in the superconductor and limited coexistence with the f_0 triplet correlations.

Next, Fig. 4 shows T_c as a function of the out-of-plane misalignment angle θ for differing (a) superconductor widths D_S , (b) normal layer widths D_N , and (c) spin-independent interface scattering strengths H_B . If the relative magnetizations were to rotate in-plane, the T_c behavior discussed here would be identical, thus providing additional experimental options for observing the predicted effects. In (a), the sensitivity of T_c to the S layer width is shown. The importance of having thin S layers with $d_S \sim \xi_0$ (100 in our units) is clearly seen. In essence, extremely narrow S boundaries restrict Cooper pair formation, causing the ordered superconducting state to effectively become more “fragile”, consistent with other F/S systems containing thin S layers [5]. Indeed, for the thinnest case, $D_S = 100$, superconductivity completely vanishes for most magnetization configurations, except when θ is near the parallel or antiparallel orientations. At the thickest D_S shown ($D_S = 200$), the sensitivity to θ has dramatically diminished, as pair-breaking effects from the adjacent ferromagnet now have a limited overall effect in the larger superconductor. For all S widths considered, the minimum in T_c occurs when θ lies slightly off the orthogonal configuration ($\theta = 90^\circ$), consistent with some quasiclassical systems [3]. Next, in Fig. 4(b) the S layer thickness is set to $D_S = 130$, while several nonmagnetic N metal spacer widths are

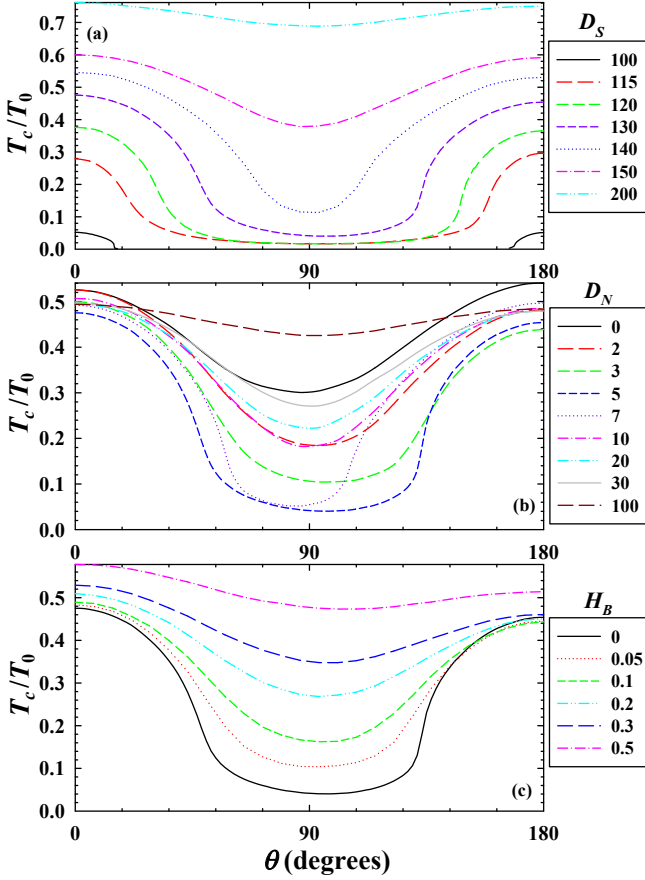


FIG. 4. (Color online). Critical temperature T_c as a function of the relative exchange field orientation angle θ . In (a) the normal metal insert has a width of $D_N = 5$, and the S width varies as shown in the legend, from $D_S=100$ to $D_S = 200$. In (b) the S width is fixed at $D_S = 130$, while the N spacer is varied. In (c) the effects of interfacial scattering are examined, with $D_S = 130$, $D_N = 5$. The legend depicts the various scattering strengths H_B considered.

considered. The presence of the N layer clearly plays a crucial role in the thermodynamics of the spin valve. Indeed, an optimum $D_N \approx 5$ exists which yields the greatest $\Delta T_c(\theta)$: Increasing or decreasing D_N around this value can significantly reduce the size of the spin valve effect. Physically, this behavior is related to the spin-triplet conversion that takes place in the ferromagnets and corresponding enhancement of the equal-spin triplet correlations in the N layer. This will be discussed in greater detail below. For D_N much larger than the optimal width, a severe reduction in magnetic interlayer coupling occurs and T_c exhibits little variation with θ . Finally, in Fig. 4(c), we incorporate spin-independent scattering at each of the spin valve interfaces. A wide range of scattering strengths are considered. We assume $H_j \equiv H$ ($j = 1, 2, 3$), so that interface scattering can be written solely in terms of the dimensionless parameter $H_B = H/v_F$. Overall, the general features and trends for T_c seen previously are retained. With mod-

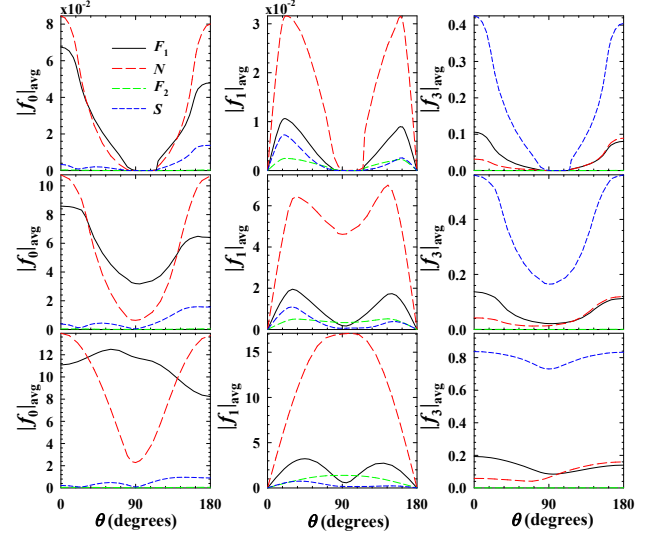


FIG. 5. (Color online). Normalized triplet (f_0 , f_1) and singlet (f_3) amplitudes versus the relative magnetization angle θ . The magnitude of each pair correlation is averaged over a given region in the SF_1NF_2 spin valve, as identified in the legend. The top, middle, and bottom rows correspond to $D_S = 130$, $D_S = 150$, and $D_S = 300$ respectively.

erate amounts of interface scattering, $H_B = 0.1$, we find $\Delta T_c \equiv T_c(\theta = 0^\circ) - T_c(\theta = 90^\circ) \approx 0.3T_0$. It is immediately evident that samples must have interfaces as transparent as possible [25, 27]: the variations in T_c with θ become severely reduced with increasing H_B , as the phase coherence of the superconducting correlations becomes destroyed. In all cases, we observe some degree of asymmetry in T_c as a function of θ , similar to what has been reported in both diffusive [3] and clean [5] spin valves lacking half-metallic elements. If it is assumed that the band splitting in F_2 is sufficiently large so that only one spin species can exist, a quasiclassical approach has shown that T_c becomes symmetric with respect to θ in the diffusive regime [30].

To correlate the large spin-valve effect observed in Fig. 4 with the odd-time triplet correlations, we employ the expressions in Eqs. (3a) and (3b), which describe the spatial and temporal behavior of the triplet amplitudes. We normalize the triplet correlations, computed in the low T limit, to the value of the singlet pair amplitude in the bulk S . The normalized averages of $|f_0|$ and $|f_1|$ are plotted as functions of θ in Fig. 5, at a dimensionless characteristic time of $\tau = 4$. For comparison purposes, the singlet pair correlations, f_3 , are also shown (third column). In each panel, spatial averages over different segments of the spin valve are displayed as separate curves (see caption). Each row of figures corresponds to different D_S : $D_S = 130, 150, 300$ (from top to bottom). One of the most striking observations is the effect of the normal metal spacer, which contains a substantial portion of the equal-spin triplet pairs. We will see below that the f_1 triplet correlations within the nor-

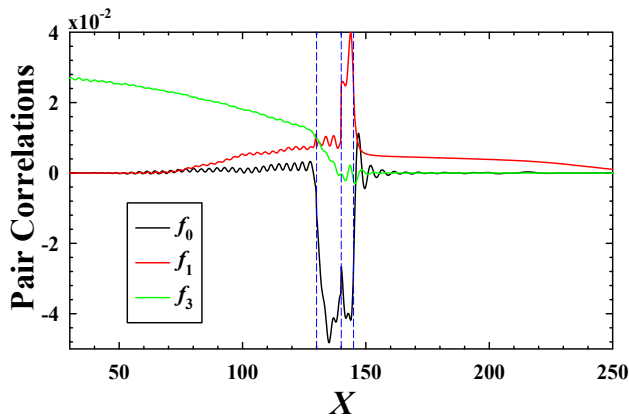


FIG. 6. (Color online). Normalized triplet (f_0 , f_1) and singlet (f_3) amplitudes versus the dimensionless coordinate X . The relative magnetization orientation is set to $\theta = 20^\circ$. The dashed vertical lines identify the locations of the interfaces for the SF_1NF_2 structure. Each segment corresponds to the following ranges: $X < 130$ (S region), $130 \leq X \leq 140$ (F_1 region), $140 < X \leq 145$ (N region), and $X > 145$ (F_2 region). The singlet component has been reduced by a factor of 10 for comparison purposes.

mal metal tend to propagate into the adjacent regions of the spin valve as time evolves. Examining the top two panels of Fig. 5, the equal-spin f_1 triplet component in S clearly dominates its opposite spin counterpart when $\theta \approx 20^\circ$. Thus, only slight deviations from the parallel state ($\theta = 0^\circ$) generates triplet correlations within S that have spin projection $m = \pm 1$. For each D_S case studied, the singlet f_3 amplitudes are clearly largest in the S region where they originate, and then decline further in each subsequent segment. It is evident also that the f_1 triplet pair amplitudes are anticorrelated to T_c (governed by the behavior of the singlet amplitudes), which indicates a singlet-triplet conversion process. Therefore as more singlet superconductivity leaks into the ferromagnet side, T_c is suppressed, and triplet superconductivity is enhanced. It is evident that both triplet components vanish around $\theta = 90^\circ$, as was also observed in Fig. 3. This is due to the highly sensitive nature of the gapless superconducting state that arises in thin S systems, whereby the singlet pair correlations become rapidly destroyed as the magnetization vector in F_1 approaches the orthogonal configuration. Increasing the size of the superconductor causes the superconducting state to become more robust to changes in θ , and consequently the system no longer transitions to a resistive state at $\theta \approx 90^\circ$. The triplet correlations reflect this aspect as seen in the middle and bottom panels of Fig. 5, whereby both triplet components have finite values for the orthogonal orientation. Overall, there is a dramatic change in both triplet components when the S part of the spin valve is increased in size. For example, the f_1 triplet correlations in N and in F_2 evolve from having two peaks to a single maximum at $\theta = 90^\circ$. The D_S trends also reflect the importance of self-consistency of the pair potential $\Delta(x)$

for thinner superconductors, where a self-consistent singlet component $f_3(x)$ can substantially decline, or vanish altogether, in contrast to simple step function. Indeed, the observed disappearance of the singlet and triplet pair correlations for thin superconductors at $\theta \simeq 90^\circ$ (see top panels), can only occur if the pair potential is calculated self-consistently [Eq. (2)], thus ensuring that the free energy of the system is lowest [36]. As will be seen below, this important step permits the proper description of the proximity effects leading to nontrivial spatial behavior of $\Delta(x)$ in and around the interfaces for both the superconductor and ferromagnets [44]. In common non self-consistent approaches, where $\Delta(x)$ is treated phenomenologically as a prescribed constant in the S region, this vital behavior is lost.

Next, in Fig. 6 we present the spatial behavior of the real parts of the triplet and singlet pair correlations throughout each segment of the spin valve. We choose $\theta = 20^\circ$ in order to optimize the f_1 triplet component in S . The other parameters used correspond to $D_S = 130$, $D_N = 5$, and $T = 0.05$. Proximity effects are seen to result in a reduction of the singlet f_3 correlations in the S region near the interface at $X = 130$. As usual, this decay occurs over the coherence length ξ_0 . The singlet amplitude then declines within the F_1 region before undergoing oscillations and quickly dampening out in the half-metal. Thus, as expected, the singlet Cooper pairs cannot be sustained in the half-metallic segment where only one spin species exists. Within the half-metal, the triplet component, f_0 (also comprised of opposite-spin pairs), undergoes damped oscillations similar to the f_3 correlations. It is notable that the triplet f_0 component is severely limited in the S region, in stark contrast to the singlet correlations. Therefore, the f_0 correlations in this situation are confined mainly to the F_1 and N regions. The equal-spin f_1 triplet component on the other hand, is seen to pervade every segment of the spin valve: The f_1 correlations are enhanced in the N region, similar in magnitude to f_0 , but then exhibit a slow decay in both the S and half-metallic regions.

To further clarify the role of the triplet correlations in the spin valve, we now discuss the explicit relative time evolution of the triplet states in Fig. 7. Snapshots of the real parts of the triplet amplitudes are shown in equal increments of the relative time parameter τ . The angle θ is fixed at $\theta = 20^\circ$, again corresponding to when the triplet correlations with $m = \pm 1$ projection of the z -component of the total spin in the superconductor is largest (see Fig. 5). The spatial range shown permits visualization of both triplet components throughout much of the system. Starting at the earliest time $\tau = 0.8$, we find that f_1 mainly populates the nonmagnetic N region, and then as τ increases, propagates into the F_1 and F_2 regions before extending into the superconductor (left of the dashed vertical line). Meanwhile, f_0 is essentially confined to the F_1 and N regions, with limited presence in the S and F_2 layers. Since the characteristic length ξ_F over which the f_0 correlations modulate in F_2 is inversely proportional to

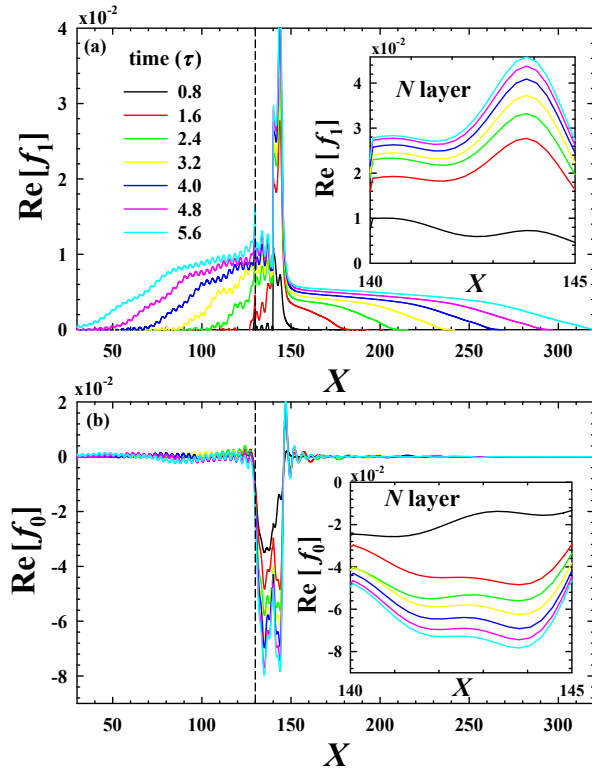


FIG. 7. (Color online). Time evolution of the localized spatial dependence of the f_0 and f_1 triplet correlations. The insets depict magnifications of the N regions ($140 \leq X \leq 145$). The dimensionless time parameter $\tau \equiv \omega_D t$ varies from 0.8 to 5.6 in increments of 0.8. Initially, the f_1 component predominately populates the N region, and then progressively moves outward into each segment of the spin valve with increasing time. The f_0 component initially occupies the F_1 and N layers, and then remains confined to those regions at higher τ . Each dashed vertical line identifies the S interface.

h_2 , f_0 declines sharply in the half-metallic region. Also, in agreement with Fig. 5, for $\theta = 20^\circ$ and $D_S = 130$, there is also a limited presence of f_0 in the superconductor. The superconductor therefore has $|f_1| \gg |f_0|$, which by using the appropriate experimental probe, can reveal signatures detailing the presence of equal-spin pairs f_1 [22].

B. Density of States

To explore these proximity induced signatures further, we investigate the experimentally relevant local DOS. An important spectroscopic tool for exploring proximity effects on an atomic scale with sub-meV energy resolution is the scanning tunneling microscope (STM). We are interested in determining the local DOS in the outer S segment of the SF_1NF_2 spin valve. By positioning a non-magnetic STM tip at the edge of the S region, the tunneling current (I) and voltage (V) characteristics can be measured [22]. This technique yields a direct probe of the

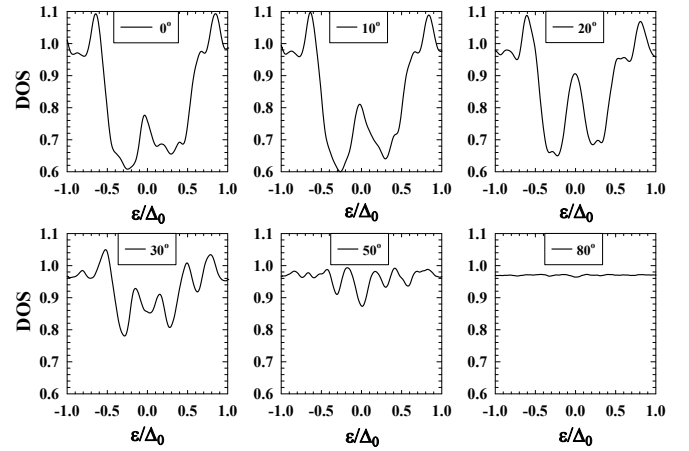


FIG. 8. (Color online). Signatures of equal-spin triplet correlations: The normalized local DOS in the superconductor for various relative magnetization orientations, θ . In the range $0^\circ \leq \theta \leq 20^\circ$, the DOS possesses peaks at zero energy which grow until they become inverted at $\theta = 30^\circ$. The well defined, prominent ZEP at $\theta = 20^\circ$ corresponds to the maximal generation of equal-spin triplet amplitudes in the S region, as shown in Fig. 5.

available electronic states with energy eV near the tip. The corresponding differential conductance $dI(V)/dV$ over the energy range of interest is then proportional to the local DOS. The vast majority of past works only considered the DOS in the ferromagnet side where the f_1 correlations were expected to dominate [22, 24, 27]. However unavoidable experimental issues related to noise and thermal broadening can yield inconclusive data. As we have shown above, with the proper alignment of relative magnetizations, one can generate a finite f_1 in S accompanied by relatively limited f_0 , thus presenting an opportunity to detect the important triplet pairs with spin $s = \pm 1$. By avoiding comparable admixtures of the two triplet components, experimental signatures of the equal-spin triplet correlations should be discernible. To investigate this further, the six panels in Fig. 8 show the normalized DOS evaluated near the edge of the superconductor for a wide variety of orientation angles θ . All plots are normalized to the corresponding value in a bulk sample of S material in its normal state. As shown, each panel ranges from a mutually parallel ($\theta = 0^\circ$) to a nearly orthogonal magnetization state ($\theta = 80^\circ$). In each case considered, we again have $D_N = 5$ and $D_S = 130$. Examining the top row of panels, traces are seen of the well-known BCS peaks that have now been shifted to subgap energies due to proximity and size effects. There also exists bound states at low energies that arise from quasiparticle interference effects. By sweeping the angle θ from the relative parallel case ($\theta = 0^\circ$) to slightly out of plane ($\theta = 20^\circ$), the zero energy quasiparticle states become significantly more pronounced. This follows from the fact that strong magnets tend to shift the relative magnetizations leading to maximal f_1 generation away

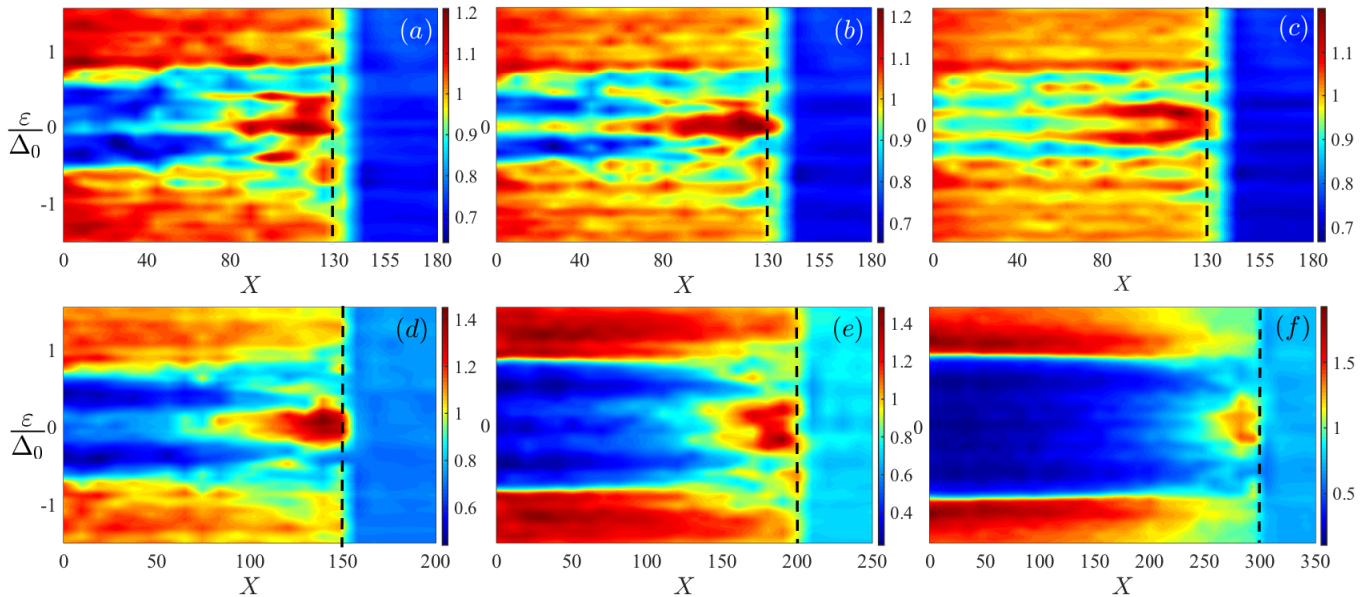


FIG. 9. (Color online). Top panels: The normalized spatially and energy resolved DOS at three different orientations of the relative magnetization angle: (a) $\theta = 10^\circ$, (b) $\theta = 20^\circ$, and (c) $\theta = 30^\circ$. Panels (a)-(c) pertain to a single system with a narrow S layer of width $D_S = 130$. The spatial region extending from $X = 0$ to 130 therefore corresponds to the superconducting region, and $X > 130$ pertains to the remaining layers of the spin valve. Bottom panels: the DOS is shown for three different S layer thicknesses: (d) $D_S = 150$, (e) $D_S = 200$, and (f) $D_S = 300$, where θ is now fixed at 20° . The dashed vertical lines identify the interface between S and F_1 .

from the expected orthogonal alignment at $\theta = 90^\circ$ [27]. The top panels reflect the gapless superconducting state often found in F/S heterostructures [45], superimposed with the triplet induced zero-energy peaks. The modifications to the superconducting state in the form of a subgap DOS in the superconductor is another signature that is indicative of the presence of spin-triplet pair correlations [22]. Finally, as θ rotates further out of plane ($\theta > 20^\circ$), the former ZEP's become inverted and vanish when $\theta = 80^\circ$, exhibiting a relatively flat DOS where the system has essentially transitioned to the normal state (see Fig. 4).

A complimentary global view of the above phenomena is presented in Fig. 9, where both the spatially and energy resolved DOS is shown at various θ (top panels) and D_S (bottom panels). The top panels (a)-(c) depict the DOS for the same parameters and normalizations used in Fig. 8, and at three orientations: $\theta = 0^\circ, 10^\circ, 20^\circ$. It is evident that increasing the misalignment angle θ , causes the ZEP in the S region to become enhanced, reaching its maximum at $\theta \approx 20^\circ$. At this angle the ZEP extends through much of the system, including to a small extent, the F_2 side. However, within S , the ZEP is clearly more dominant [22]. For the bottom panels, (d)-(f), the relative magnetization orientation is fixed at $\theta = 20^\circ$, and three larger S layers are shown: $D_S = 150$, $D_S = 200$, and $D_S = 300$. Increasing the S layer widths illustrates the ZEP evolution towards a familiar gapped DOS of a BCS form. As seen, the ZEP is maximal in the superconducting region near the S/F_1 interface. By increasing

D_S , the ZEP in the S side becomes diminished until for sufficiently large D_S , that is, $D_S \approx 200$, the well-known singlet superconducting gap begins to emerge throughout much of the superconductor. At an even larger D_S ($D_S = 300$), the ZEP has clearly weakened even further. Finally, for the experiment reported in Ref. 25, a peak in the resistive transitions at external fields of $B > 0.25$ T was observed immediately before the critical temperature whereby the system has transitioned to the superconducting phase. This peak in the transition curves was believed to be caused by the influence of the external field, effectively creating a $SF_1F'F_2$ type of configuration. We investigated such a configuration for various strengths and orientations of the F' ferromagnet, and no evidence was found that was suggestive of anomalous behavior near T_c for F' with weak exchange fields. Note that the system under consideration is translationally invariant in the yz plane (see Fig. 1). Therefore, the spin valve structure may experience a Fulde Ferrell-Larkin-Ovchinnikov phase during its phase transition from the superconducting to normal phase, although in a narrow region of parameter space [54, 55].

C. Spin Currents

To reveal further details of the exchange interaction which controls the behavior and type of triplet correlations present in the system, we next examine the characteristics of the spin currents that exist within the spin

valve. When the magnetizations in F_1 and F_2 are non-collinear, the exchange interaction in the ferromagnets creates a spin current \mathbf{S} that flows in parts of the system, even in the absence of a charge current. If the spin current varies spatially, the corresponding nonconserved spin currents in F_1 and F_2 generate a mutual torque that tends to rotate the magnetizations of the two ferromagnets. This process is embodied in the spin-torque continuity equation [50, 51] which describes the time evolution of the spin density $\boldsymbol{\eta}$:

$$\frac{\partial}{\partial t} \langle \eta_i(x) \rangle + \frac{\partial}{\partial x} S_i(x) = \tau_i(x), \quad i = x, y, z, \quad (5)$$

where $\boldsymbol{\tau}(x)$ is the spin transfer torque (STT): $\boldsymbol{\tau}(x) = -(2/\mu_B) \mathbf{m}(x) \times \mathbf{h}(x)$, $\mathbf{m}(x)$ is the magnetization, and μ_B is the Bohr magneton (see Appendix A). The spin current tensor here has been reduced to vector form due to the quasi-one dimensional nature of the geometry. We calculate $\mathbf{S}(x)$ by performing the appropriate sums of quasi-particle amplitudes and energies [see Eq. (A10)]. In the steady state, the continuity equation, Eq. (5), determines the torque by simply evaluating the derivative of the spin current as a function of position: $\tau_i(x) = \partial S_i(x)/\partial x$. The net torque acting within the boundaries of e.g., the F_1 layer, is therefore the change in spin current across the two interfaces bounding that region:

$$S_y(d_S + d_{F_1}) - S_y(d_S) = \int_{F_1} dx \tau_y. \quad (6)$$

In equilibrium, the net τ_y in F_2 is opposite to its counterpart in F_1 . Since no spin current flows in the superconductor, we have $S_y(d_S) = 0$, and the net torque in F_1 is equivalent to the spin current flowing through N .

In our setup, the exchange field in F_1 is directed in the $x - z$ plane, and therefore the spin current and torque are directed orthogonal to this plane (along the interfaces in the y direction). Likewise, if the magnetizations were varied in the $y - z$ plane, the spin currents would be directed along x . Figure 10 thus illustrates the normalized spin current S_y as a function of the dimensionless position X . The normalization factor S_0 is written in terms of $n_e v_F$, where $n_e = k_F^3/(3\pi^2)$, and $v_F = k_F/m$. Several equally spaced magnetization orientations θ are considered, ranging from parallel ($\theta = 0^\circ$), to orthogonal ($\theta = 90^\circ$). Within the two F regions, S_y tends to undergo damped oscillations, while in N there is no exchange interaction ($\mathbf{h} = 0$), and consequently the spin current is constant for a given θ . The main plot shows that when $\theta = 0^\circ$, S_y vanishes throughout the entire system, as expected for parallel magnetizations. By varying θ , spin currents are induced due to the misaligned magnetic moments in the F layers. If the exchange field is rotated slightly out of plane, such that $\theta \lesssim 30^\circ$, it generates on average, negative spin currents in the N and F_1 regions. As shown, these spin currents reverse their polarization direction for larger θ . This behavior is consistent with the inset, which shows how tuning θ affects S_y

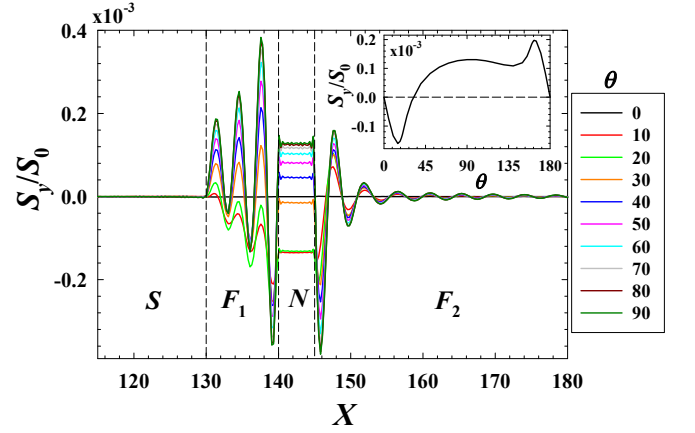


FIG. 10. (Color online). Spin current S_y as a function of position X in the spin valve. Several magnetization orientations θ are considered as shown in the legend. The dashed vertical lines identify the interfaces of each layer as labeled. The inset corresponds to the spin current within the N region.

(or equivalently, the net torque) in N . Thus, by manipulating θ , the strength and direction of the spin current in the normal metal can be controlled, or even eliminated completely at $\theta \approx 34^\circ$. By varying θ about this angle, the overall torque, which tends to align the magnets in a particular direction, can then reverse in a given magnet. For $\theta \approx 15^\circ$ and $\theta \approx 160^\circ$, the inset also clearly shows an enhancement of the magnitude of the spin currents, which coincides approximately to the orientations leading to an increase in the spin-polarized triplet pairs observed in Fig. 5.

In conclusion, motivated by recent experiments [22, 25], a hybrid SF_1NF_2 spin valve containing a half-metallic ferromagnet has been theoretically investigated, revealing a sizable spin-valve effect for thin superconductors with widths close to ξ_0 . Through self-consistent numerical calculations, the contributions from both the equal-spin (f_1) and opposite-spin (f_0) triplet correlations have been identified as the relative magnetization angle θ varies. We found that when the magnetization in F_1 is directed slightly out-of-plane, the magnitude of f_1 in S is maximized, while for f_0 it is very small. By investigating the DOS in the superconductor over a broad range of θ , we were able to identify the emergence of zero energy peaks (ZEPs) in the DOS that coincide with peaks in the averaged $|f_1|$. Our results show, to a large extent, good agreement with experimental observations as well as the physical origins of these effects. We have thus established a clear, experimentally identifiable role that the triplet correlations play in this new class of half-metallic spin valve structures. For future work, it would be interesting to study the transport properties of these types of spin valves by investigating the self-consistent charge and spin currents as they pertain to dissipationless spintronics applications.

III. ACKNOWLEDGEMENTS

This work was supported in part by ONR and a grant of HPC resources from the DOD HPCMP. We thank N. Birge for a careful reading of the manuscript and helpful comments.

Appendix A: Spin Currents

In order to calculate the spin currents flowing within the spin valve, it is convenient to employ the Heisenberg picture to determine the time evolution of the spin density, $\boldsymbol{\eta}(\mathbf{r}, t)$,

$$\frac{\partial}{\partial t} \langle \boldsymbol{\eta}(\mathbf{r}, t) \rangle = i \langle [\mathcal{H}_{\text{eff}}, \boldsymbol{\eta}(\mathbf{r}, t)] \rangle, \quad (\text{A1})$$

where $\boldsymbol{\eta}(\mathbf{r})$ is the spin density operator defined as,

$$\boldsymbol{\eta}(\mathbf{r}) = \psi^\dagger(\mathbf{r}) \boldsymbol{\sigma} \psi(\mathbf{r}). \quad (\text{A2})$$

We define the effective BCS Hamiltonian [36], \mathcal{H}_{eff} , via

$$\begin{aligned} \mathcal{H}_{\text{eff}} = \int d^3r \Big\{ & \psi^\dagger(\mathbf{r}) [\mathcal{H}_0(\mathbf{r}) - \mathbf{h}(\mathbf{r}) \cdot \boldsymbol{\sigma}] \psi(\mathbf{r}) \\ & + \Delta(\mathbf{r}) \psi_\uparrow^\dagger(\mathbf{r}) \psi_\downarrow^\dagger(\mathbf{r}) + \Delta^*(\mathbf{r}) \psi_\downarrow(\mathbf{r}) \psi_\uparrow(\mathbf{r}) \Big\}, \end{aligned} \quad (\text{A3})$$

where $\psi_\sigma^\dagger(\mathbf{r}), \psi_\sigma(\mathbf{r})$ denotes the fermionic field operators with spin projections $\sigma = \uparrow, \downarrow$ along a given quantization axis, and $\boldsymbol{\sigma}$ is the usual vector of Pauli matrices. Inserting the Hamiltonian, Eq. (A3), into (A1) yields the following continuity equation:

$$\frac{\partial}{\partial t} \langle \boldsymbol{\eta}(\mathbf{r}, t) \rangle + \frac{\partial \mathbf{S}}{\partial x} = \boldsymbol{\tau}, \quad (\text{A4})$$

where \mathbf{S} is the spin current which in our geometry is a vector (in general it is a tensor). The spin-transfer torque, $\boldsymbol{\tau}$, is given by:

$$\boldsymbol{\tau} = -i \langle \psi^\dagger(\mathbf{r}) [\mathbf{h} \cdot \boldsymbol{\sigma}, \boldsymbol{\sigma}] \psi(\mathbf{r}) \rangle = 2 \langle \psi^\dagger(\mathbf{r}) [\boldsymbol{\sigma} \times \mathbf{h}] \psi(\mathbf{r}) \rangle. \quad (\text{A5})$$

Recalling the expression for the local magnetization, $\mathbf{m}(\mathbf{r})$,

$$\mathbf{m}(\mathbf{r}) = -\mu_B \langle \boldsymbol{\eta}(\mathbf{r}) \rangle, \quad (\text{A6})$$

this permits the torque in Eq. (A5) to be written as,

$$\boldsymbol{\tau} = 2 \langle \psi^\dagger(\mathbf{r}) \boldsymbol{\sigma} \psi(\mathbf{r}) \rangle \times \mathbf{h} = -\frac{2}{\mu_B} \mathbf{m} \times \mathbf{h}. \quad (\text{A7})$$

In the steady state, and when a torque is present, the spin current therefore must have at least one spatially varying component. After taking the commutator in Eq. (A1), the explicit expression for the spin-current is found to be,

$$\mathbf{S} = -\frac{i}{2m} \left\langle \psi^\dagger(\mathbf{r}) \boldsymbol{\sigma} \frac{\partial \psi(\mathbf{r})}{\partial x} - \frac{\partial \psi^\dagger(\mathbf{r})}{\partial x} \boldsymbol{\sigma} \psi(\mathbf{r}) \right\rangle, \quad (\text{A8})$$

where for our quasi-one-dimensional systems, the vector \mathbf{S} represents the spin current flowing along the x direction with spin components (S_x, S_y, S_z) . To write the spin current in terms of the calculated quasiparticle amplitudes and energies, the field operators are directly expanded by means of a Bogoliubov transformation [36]:

$$\psi_\uparrow(\mathbf{r}) = \sum_n (u_{n\uparrow}(\mathbf{r}) \gamma_n - v_{n\uparrow}^*(\mathbf{r}) \gamma_n^\dagger), \quad (\text{A9a})$$

$$\psi_\downarrow(\mathbf{r}) = \sum_n (u_{n\downarrow}(\mathbf{r}) \gamma_n + v_{n\downarrow}^*(\mathbf{r}) \gamma_n^\dagger), \quad (\text{A9b})$$

where $u_{n\sigma}$ and $v_{n\sigma}$ are the quasiparticle and quasihole amplitudes, and γ_n and γ_n^\dagger are the Bogoliubov quasiparticle annihilation and creation operators, respectively. By directly considering the commutation relations for the quantum mechanical operators, the following expectation values must be satisfied throughout our calculations: $\langle \gamma_n^\dagger \gamma_m \rangle = \delta_{nm} f_n$, $\langle \gamma_m \gamma_n^\dagger \rangle = \delta_{nm} (1 - f_n)$, and $\langle \gamma_n \gamma_m \rangle = 0$. Here f_n is the Fermi function which depends on the temperature T and quasiparticle energy ε_n : $f_n = (\exp[\varepsilon_n/(2T)] + 1)^{-1}$. We can now expand each spin component of the spin current in terms of the quasiparticle amplitudes to obtain [50, 51]:

$$S_x = -\frac{i}{2m} \sum_n \left\{ f_n \left[u_{n\uparrow}^* \frac{\partial u_{n\downarrow}}{\partial x} + u_{n\downarrow}^* \frac{\partial u_{n\uparrow}}{\partial x} - u_{n\downarrow} \frac{\partial u_{n\uparrow}^*}{\partial x} - u_{n\uparrow} \frac{\partial u_{n\downarrow}^*}{\partial x} \right] - (1 - f_n) \left[v_{n\uparrow} \frac{\partial v_{n\downarrow}^*}{\partial x} + v_{n\downarrow} \frac{\partial v_{n\uparrow}^*}{\partial x} - v_{n\uparrow}^* \frac{\partial v_{n\downarrow}}{\partial x} - v_{n\downarrow}^* \frac{\partial v_{n\uparrow}}{\partial x} \right] \right\}, \quad (\text{A10})$$

$$S_y = -\frac{1}{2m} \sum_n \left\{ f_n \left[u_{n\uparrow}^* \frac{\partial u_{n\downarrow}}{\partial x} - u_{n\downarrow}^* \frac{\partial u_{n\uparrow}}{\partial x} - u_{n\downarrow} \frac{\partial u_{n\uparrow}^*}{\partial x} + u_{n\uparrow} \frac{\partial u_{n\downarrow}^*}{\partial x} \right] - (1 - f_n) \left[v_{n\uparrow} \frac{\partial v_{n\downarrow}^*}{\partial x} - v_{n\downarrow} \frac{\partial v_{n\uparrow}^*}{\partial x} + v_{n\uparrow}^* \frac{\partial v_{n\downarrow}}{\partial x} - v_{n\downarrow}^* \frac{\partial v_{n\uparrow}}{\partial x} \right] \right\}, \quad (\text{A11})$$

$$S_z = -\frac{i}{2m} \sum_n \left\{ f_n \left[u_{n\uparrow}^* \frac{\partial u_{n\uparrow}}{\partial x} - u_{n\uparrow} \frac{\partial u_{n\uparrow}^*}{\partial x} - u_{n\downarrow}^* \frac{\partial u_{n\downarrow}}{\partial x} + u_{n\downarrow} \frac{\partial u_{n\downarrow}^*}{\partial x} \right] - (1 - f_n) \left[-v_{n\uparrow} \frac{\partial v_{n\uparrow}^*}{\partial x} + v_{n\uparrow}^* \frac{\partial v_{n\uparrow}}{\partial x} + v_{n\downarrow} \frac{\partial v_{n\downarrow}^*}{\partial x} - v_{n\downarrow}^* \frac{\partial v_{n\downarrow}}{\partial x} \right] \right\}. \quad (\text{A12})$$

In the case of F layers with uniform magnetization, there is no net spin current. The introduction of an inhomogeneous magnetization texture however results in a net spin current imbalance that is finite even in the absence of a charge current.

-
- [1] M. Eschrig, *Spin-polarized supercurrents for spintronics: a review of current progress*, *Reports on Progress in Physics* **78**, 104501 (2015).
- [2] J. Linder, J.W.A. Robinson, *Superconducting Spintronics*, *Nat. Phys.* **11**, 307 (2015).
- [3] Ya. V. Fominov, A. A. Golubov, T. Yu. Karminskaya, M. Yu. Kupriyanov, R. G. Deminov, L. R. Tagirov, *Superconducting triplet spin valve*, *JETP Letters* **91**, 308 (2010).
- [4] T. Y. Karminskaya, A. A. Golubov, and M. Y. Kupriyanov, *Anomalous proximity effect in spin-valve superconductor/ferromagnetic metal/ferromagnetic metal structures*, *Phys. Rev. B* **84**, 064531 (2011).
- [5] C. T. Wu, O. T. Valls, and K. Halterman, *Proximity effects and triplet correlations in Ferromagnet/Ferromagnet/Superconductor nanostructures*, *Phys. Rev. B* **86**, 014523 (2012).
- [6] P.V. Leksin, N. N. Garif'yanov, I. A. Garifullin, Ya. V. Fominov, J. Schumann, Y. Krupskaya, V. Kataev, O. G. Schmidt, and B. Büchner, *Evidence for Triplet Superconductivity in a Superconductor-Ferromagnet Spin Valve*, *Phys. Rev. Lett.* **109**, 057005 (2012).
- [7] M. Eschrig, T. Lofwander, *Triplet supercurrents in clean and disordered half-metallic ferromagnets*, *Nat. Phys.* **4**, 138 (2008).
- [8] F. S. Bergeret, A. F. Volkov, and K. B. Efetov, *Odd triplet superconductivity and related phenomena in superconductor-ferromagnet structures*, *Rev. Mod. Phys.* **77**, 1321 (2005).
- [9] A. I. Buzdin, *Proximity effects in superconductor-ferromagnet heterostructures* *Rev. Mod. Phys.* **77**, 935-936 (2005).
- [10] R. S. Keizer, S. T. B. Goennenwein, T. M. Klapwijk, G. Miao, G. Xiao and A. Gupta, *A spin triplet supercurrent through the half-metallic ferromagnet CrO₂* *Nature* **439**, 825 (2006).
- [11] I. V. Bobkova and A. M. Bobkov, *Long-range proximity effect for opposite-spin pairs in superconductor-ferromagnet heterostructures under nonequilibrium quasiparticle distribution*, *Phys. Rev. Lett.* **108**, 197002 (2012).
- [12] A. Moor, A. F. Volkov, K. B. Efetov, *Nematic versus ferromagnetic spin filtering of triplet Cooper pairs in superconducting spintronics*, *Phys. Rev. B* **92**, 180506(R) (2015).
- [13] Y.N. Khaydukov, G.A. Ovsyannikov, A.E. Sheyerman, K.Y. Constantinian, L. Mustafa, T. Keller, M.A. Uribe-Laverde, Yu.V. Kisilinskii, A.V. Shadrin, A. Kalabukhov, B. Keimer, D. Winkler, *Evidence for spin-triplet superconducting correlations in metal-oxide heterostructures with noncollinear magnetization*, *Phys. Rev. B* **90**, 035130 (2014).
- [14] M. Alidoust and K. Halterman, *Proximity induced vortices and long-range triplet supercurrents in ferromagnetic Josephson junctions and spin valves*, *J. Appl. Phys.* **117**, 123906 (2015).
- [15] K. Halterman, O. T. Valls, and P. H. Barsic, *Induced triplet pairing in clean s-wave superconductor/ferromagnet layered structures* *Phys. Rev. B* **77**, 174511 (2008).
- [16] K. Halterman, P. H. Barsic, and O. T. Valls, *Odd Triplet Pairing in Clean Superconductor/Ferromagnet Heterostructures* *Phys. Rev. Lett.* **99**, 127002 (2007).
- [17] I. Baladie, A.I. Buzdin, *Local quasiparticle density of states in ferromagnet/superconductor nanostructures*, *Phys. Rev. B* **64**, 224514 (2001).
- [18] F.S. Bergeret, A.F. Volkov, K.B. Efetov, *Local density of states in superconductor/strong ferromagnet structures*, *Phys. Rev. B* **65**, 134505 (2002).
- [19] S. V. Bakurskiy, N. V. Klenov, I. I. Soloviev, M. Yu. Kupriyanov and A. A. Golubov, *Superconducting phase domains for memory applications*, *Appl. Phys. Lett.* **108**, 042602 (2016).
- [20] S.V. Bakurskiy, N.V. Klenov, I.I. Soloviev, V.V. Bolginov, V.V. Ryazanov, I.V. Vernik, O.A. Mukhanov, M.Yu. Kupriyanov and A.A. Golubov, *Theoretical model of superconducting spintronic SIFS devices*, *Appl. Phys. Lett.* **102**, 192603 (2013).
- [21] T. Yu. Karminskaya, M. Yu. Kupriyanov, S. L. Prischepa, and A. A. Golubov, *Conductance spectroscopy in ferromagnet/superconductor hybrids*, *Supercond. Sci. Technol.* **27**, 075008 (2014).
- [22] Y. Kalcheim, O. Millo, A. Di Bernardo, A. Pal, and J. W. A. Robinson, *Inverse proximity effect at superconductor-ferromagnet interfaces: Evidence for induced triplet pairing in the superconductor*, *Phys. Rev. B* **92**, 060501 (2015).
- [23] G. Nowak, H. Zabel, K. Westerholt, I. Garifullin, M. Marcellini, A. Liebig, and B. Hjörvarsson, *Superconducting spin valves based on epitaxial Fe/V superlattices*, *Phys. Rev. B* **78**, 134520 (2008).
- [24] S. Kawabata, Y. Asano, Y. Tanaka, and A. A. Golubov, *Robustness of Spin-Triplet Pairing and Singlet-Triplet Pairing Crossover in Superconductor/Ferromagnet Hybrids*, *J. Phys. Soc. Jap.* **82**, 124702 (2013).
- [25] A. Singh, S. Voltan, K. Lahabi, and J. Aarts, *Colossal Proximity Effect in a Superconducting Triplet Spin Valve Based on the Half-Metallic Ferromagnet CrO₂*, *Phys. Rev. X* **5**, 021019 (2015).
- [26] V. Braude and Yu. V. Nazarov, *Fully Developed Triplet Proximity Effect*, *Phys. Rev. Lett.* **98**, 077003 (2007).
- [27] M. Alidoust, K. Halterman, and O. T. Valls *Zero Energy Peak and Triplet Correlations in Nanoscale SFF Spin-Valves*, *Phys. Rev. B* **92**, 014508 (2015).
- [28] T. Yokoyama, Y. Tanaka, A. A. Golubov, *Manifestation of the odd-frequency spin-triplet pairing state in diffusive ferromagnet/superconductor junctions*, *Phys. Rev. B* **75**, 134510 (2007).
- [29] M. Eschrig, A. Cottet, W. Belzig, and J. Linder, *General boundary conditions for quasiclassical theory of superconductivity in the diffusive limit: application to strongly spin-polarized systems*, *New. J. Phys.* **17**, 083037 (2015).

- [30] S. Mironov, A. Buzdin, *Triplet proximity effect in superconducting heterostructures with a half-metallic layer*, *Phys. Rev. B* **92**, 184506 (2015).
- [31] A. Di Bernardo, Z. Salman, X.L. Wang, M. Amado, M. Egilmez, M.G. Flokstra, A. Suter, S.L. Lee, J.H. Zhao, T. Prokscha, E. Morenzoni, M.G. Blamire, J. Linder and J.W.A. Robinson, *Intrinsic Paramagnetic Meissner Effect Due to s-Wave Odd-Frequency Superconductivity*, *Phys. Rev. X* **5**, 041021 (2015).
- [32] M. Alidoust, K. Halterman and J. Linder, *Meissner effect probing of odd-frequency triplet pairing in superconducting spin valves*, *Phys. Rev. B* **89**, 054508 (2014).
- [33] J. Zhu, I. N. Krivorotov, K. Halterman, and O. T. Valls *Angular Dependence of the Superconducting Transition Temperature in Ferromagnet-Superconductor-Ferromagnet Trilayers*, *Phys. Rev. Lett.* **105**, 207002 (2010).
- [34] A. A. Jara, C. Safranski, I. N. Krivorotov, C.-T. Wu, A. N. Malmi-Kakkada, O. T. Valls, and K. Halterman, *Angular dependence of superconductivity in superconductor / spin valve heterostructures*, *Phys. Rev. B* **89**, 184502 (2014)s.
- [35] K. Westerholt, D. Sprungmann, H. Zabel, R. Brucas, B. Hjörvarsson, D. A. Tikhonov, and I. A. Garifullin, *Superconducting Spin Valve Effect of a V Layer Coupled to an Antiferromagnetic [Fe/V] Superlattice*, *Phys. Rev. Lett.* **95**, 097003 (2005).
- [36] P.G. de Gennes, *Superconductivity of Metals and Alloys*, (Addison-Wesley, reading, Massachussetts, 1989).
- [37] J. Wang, M. Singh, M. Tian, N. Kumar, B. Liu, C. Shi, J. K. Jain, N. Samarth, T. E. Mallouk, and M. H. W. Chan, *Interplay between superconductivity and ferromagnetism in crystalline nanowires* *Nat. Phys.* **6**, 389 (2010).
- [38] C. Visani, Z. Sefrioui, J. Tornos, C. Leon, J. Briatico, M. Bibes, A. Barthelémy, J. Santamaría, and Javier E. Villegas, *Equal-spin Andreev reflection and long-range coherent transport in high-temperature superconductor/half-metallic ferromagnet junctions* *Nature Phys.* **8** 539 (2012).
- [39] Z. Radović, M. Ledvij, L. Dobrosavljevic-Grujic, A. I. Buzdin, and J. R. Clem, *Transition temperatures of superconductor-ferromagnet superlattices* , *Phys. Rev. B* **44**, 759 (1991).
- [40] J. S. Jiang, D. Davidović, Daniel H. Reich, and C. L. Chien, *Oscillatory superconducting transition temperature in Nb/Gd multilayers*, *Phys. Rev. Lett.* **74**, 314 (1995).
- [41] Y Blum, A Tsukernik, M Karpovski, A Palevski, *Oscillations of the superconducting critical current in Nb-Cu-Ni-Cu-Nb junctions*, *Phys. Rev. Lett.*, **89**, 187004 (2002).
- [42] J. Y. Gu, C.-Y. You, J. S. Jiang, J. Pearson, Ya. B. Bazaliy, and S. D. Bader, *Magnetization-Orientation Dependence of the Superconducting Transition Temperature in the Ferromagnet-Superconductor-Ferromagnet System: CuNi/Nb/CuNi*, *Phys. Rev. Lett.*, **89**, 267001 (2002).
- [43] L. R. Tagirov, *Low-field superconducting spin switch based on a superconductor/ferromagnet multilayer*, *Phys. Rev. Lett.*, **83**, 2058 (1999).
- [44] K. Halterman and O.T. Valls, *Proximity effects at ferromagnet-superconductor interfaces*, *Phys. Rev. B* **65**, 014509 (2001).
- [45] K. Halterman and O. T. Valls, *Energy gap of ferromagnet-superconductor bilayers*, *Physica C* **397** 151 (2003).
- [46] T. Tokuyasu, J. A. Sauls, and D. Rainer, *Proximity effect of a ferromagnetic insulator in contact with a superconductor*, *Phys. Rev. B* **38**, 8823 (1988).
- [47] C. T. Wu, K. Halterman, and O. T. Valls, *Proximity effects and triplet correlations in ferromagnet/ferromagnet/superconductor nanostructures*, *Phys. Rev. B* **86**, 014523 (2012).
- [48] M. S. Anwar, M. Veldhorst, A. Brinkman, and J. Aarts, *Long range supercurrents in ferromagnetic CrO₂ using a multilayer contact structures*, *Appl. Phys. Lett.* **100**, 052602 (2012).
- [49] K. Halterman and O. T. Valls, *Emergence of Triplet Correlations in Superconductor/Half Metallic Nanojunctions with Spin Active Interfaces*, *Phys. Rev B* **80**, 104502 (2009).
- [50] K. Halterman, O.T. Valls, and C.-T. Wu, *Charge and spin currents in ferromagnetic Josephson junctions*, *Phys. Rev B* **92**, 174516 (2015).
- [51] K. Halterman, and M. Alidoust, *Josephson currents and spin-transfer torques in ballistic SFSFS nanojunctions*, *Supercond. Sci. Technol.* **29**, 055007 (2016).
- [52] Y. Kalcheim, O. Millo, M. Egilmez, J. W. A. Robinson, and M. G. Blamire *Evidence for anisotropic triplet superconductor order parameter in half-metallic ferromagnetic La_{0.7}Ca_{0.3}Mn₂O proximity coupled to superconducting Pr_{1.85}Ce_{0.15}CuO₄*, *Phys. Rev. B* **85**, 104504 (2012).
- [53] E. Katzir, S. Yochelis, F. Zeides, N. Katz, Y. Kalcheim, O. Millo, G. Leituss, Y. Myasodeyov, B. Ya. Shapiro, R. Naaman, and Y. Paltiel *Increased Superconducting Transition Temperature of a Niobium Thin Film Proximity Coupled to Gold Nanoparticles Using Linking Organic Molecules*, *Phys. Rev. Lett.* **108**, 107004 (2012).
- [54] S. Mironov, A. Melnikov, and A. Buzdin, *Vanishing Meissner effect as a Hallmark of inPlane Fulde-Ferrell-Larkin-Ovchinnikov Instability in SuperconductorFerromagnet Layered Systems*, *Phys. Rev. Lett.* **109**, 237002 (2012).
- [55] I. V. Bobkova and A. M. Bobkov, *In-plane Fulde-Ferrell-Larkin-Ovchinnikov instability in a superconductornormal metal bilayer system under nonequilibrium quasiparticle distribution*, *Phys. Rev. B* **88**, 174502 (2013).